Optical Engineering

OpticalEngineering.SPIEDigitalLibrary.org

# Optical technology for detecting the decomposition products of $SF_6$: a review

Xiaoxing Zhang
Yin Zhang
Ju Tang
Zhaolun Cui
Yanglong Li
Hong Zhou
Guangdong Zhang
Junting Yang

SPIE.

Xiaoxing Zhang, Yin Zhang, Ju Tang, Zhaolun Cui, Yanglong Li, Hong Zhou, Guangdong Zhang, Junting Yang, "Optical technology for detecting the decomposition products of $SF_6$: a review," *Opt. Eng.* **57**(11), 110901 (2018), doi: 10.1117/1.OE.57.11.110901.

Optical Engineering 57(11), 110901 (November 2018)

REVIEW

# Optical technology for detecting the decomposition products of $SF_6$: a review

**Xiaoxing Zhang,[a,*] Yin Zhang,[a] Ju Tang,[a] Zhaolun Cui,[a] Yanglong Li,[a] Hong Zhou,[a] Guangdong Zhang,[b] and Junting Yang[b]**
[a]Wuhan University, School of Electrical Engineering, Wuhan, Hubei, China
[b]Gansu Electric Power Research Institute, Lanzhou, Gansu, China

**Abstract.** Studies have demonstrated that partial discharge in $SF_6$-insulated electrical equipment can cause $SF_6$ decomposition, resulting in the generation of various products. Quantitative detection of these decomposition products can be used to evaluate the state of the equipment's insulation. The use of optical methods for detecting the products has many advantages, such as high precision, fast response, and sample reusability. Thus far, optical detection methods have been applied for detection of $SF_6$ decomposition products, and a few promising results have been obtained. We review the various optical technologies for detection of $SF_6$ decomposition products, introduce their principles and applications, and summarize some recent research progress. In addition, we propose two optical detection technologies that can be applied in this field.  [DOI: 10.1117/1.OE.57.11.110901]

Keywords: $SF_6$-insulated electrical equipment; $SF_6$ decomposition products; optical detection methods; principle; progress.

Paper 180828V received Jun. 9, 2018; accepted for publication Oct. 30, 2018; published online Nov. 16, 2018.

## 1 Introduction

Sulfur hexafluoride ($SF_6$) is a reliable insulating gas and has excellent arc-extinguishing properties. $SF_6$-insulated electrical equipment, such as switchgear, transformers, and lines, is widely used in city power grids and ultrahigh-voltage power transmission systems owing to its small footprint, high reliability, and long service life. Safe and stable operation of $SF_6$-insulated electrical equipment is crucial for effective power supply. However, during the production, installation, and maintenance of $SF_6$-insulated electrical equipment, insulation defects such as burrs and metal particles inevitably appear inside the equipment. Over long-term operation, these defects lead to partial discharge (PD). PD can cause decomposition of $SF_6$ gas, resulting in the production of various low-fluorine sulfides, such as $SF_4$, $SF_3$, $SF_2$, and $S_2F_{10}$.[1–3] Because of the presence of trace impurities, such as $H_2O$ and $O_2$, in the equipment, these low-fluorine sulfides generate many more stable decomposition products, such as $SOF_2$, $SO_2F_2$, $SO_2$, and $H_2S$. Simultaneously, PD damages the solid insulation of the equipment, causing it to react with $SF_6$ to produce $CS_2$, $CF_4$, and other decomposition products.[4–6] Without accurate detection of these products, defects in the equipment cannot be detected early. PD gradually develops and leads to deterioration of the equipment's insulation. Eventually, its effects may even threaten the safe operation of the entire power grid.

Extant studies show that the components and formation rates of $SF_6$ decomposition products due to different types of insulation defects are related to the insulation defect type and its severity.[7,8] The detection of $SF_6$ decomposition products can help in assessment of the type and severity of insulation defects. Therefore, researchers in power industry hope to adopt effective detection of $SF_6$ decomposition products to ensure timely detection of insulation defects in the equipment.[9–13]

The methods of $SF_6$ decomposition products detection can be divided into chemical and optical methods. Chemical detection employs adsorption, separation, and other methods and the various physical and chemical properties of different products to detect decomposition product concentrations. The commonly used chemical detection methods are gas chromatography (GC), detection tubes, and gas sensitivity sensors, as listed in Table 1.[14–20]

GC with high sensitivity is costly, time-consuming, and suitable for laboratory-based analysis rather than continuous on-line monitoring or portable detection. A detection tube can be used to detect major decomposition products, such as $SO_2$ or HF, at parts per million (ppm) levels. However, detection tubes have poor accuracy because the concentration of decomposition products is determined by color changes, making these tubes unsuitable for on-line monitoring.[21] A gas-sensitivity sensor can be connected to the equipment to achieve online monitoring or portable detection. However, the sensor has poor gas selectivity and is easy to be contaminated.

Optical detection is based on spectral analysis technology, which has been widely used in many fields, such as environmental science, medical treatment, chemical engineering, and food science. Most $SF_6$ decomposition products have absorption characteristics in both infrared (IR) and ultraviolet (UV) spectra. In different regions, the absorption characteristics are different. For example, Fig. 1 shows the absorption spectrum of the partial decomposition products of $SF_6$ in the UV region. The strong absorption characteristic in the 190- to 210-nm band corresponds to $CS_2$. If we use UV spectroscopy to detect this product, the detection precision can be improved. However, in the 190- to 210-nm band, interference from $H_2S$ and $SO_2$ is present and must be eliminated. Figure 2 shows the absorption spectrum of the partial decomposition products of $SF_6$ in the IR region. There is very little overlap among the spectra of the decomposition

*Address all correspondence to: Xiaoxing Zhang, E-mail: xiaoxing.zhang@outlook.com

**Table 1** Commonly used chemical detection methods.

| Method | Accuracy | Speed | Anti-interference | Range | Portability |
|---|---|---|---|---|---|
| GC | ppb | Complex operation, slow detection speed | Strong anti-interference ability | Most decomposition products | Just suitable for laboratory testing |
| Detection tube | ppm | By color comparison, fast detection speed | Easily affected by cross-interference | Partial products, such as $SO_2$, HF, and other strong acid substances | Simple structure, easy to carry |
| Gas-sensitivity sensor | ppm | Calculate through the change of sensor resistance, fast detection speed | Poor gas selectivity, easy to be contaminated | $SO_2$, $SOF_2$, $SO_2F_2$, and $H_2S$ | Good portability |

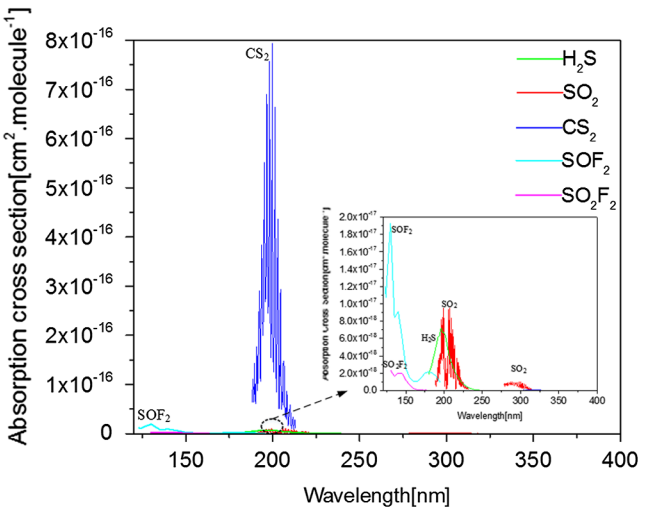


**Fig. 1** The absorption spectra of the partial decomposition of $SF_6$ in UV. All data come from The MPI-Mainz UV/VIS Spectral Atlas, which is a comprehensive collection of cross sections for gaseous molecules and radicals. $H_2S$, WuChen (1998), 295 K, 160 to 260 nm; $SO_2$, Danielache (2008), 293 K, 183 to 350 nm; $CS_2$, Ahmed Kumar (1992), 300 K, 188 to 231 nm; $SOF_2$, Pradayrol (1996), 298 K, 123 to 195 nm; $SO_2F_2$, Pradayrol (1996), 298 K, 130 to 210 nm.

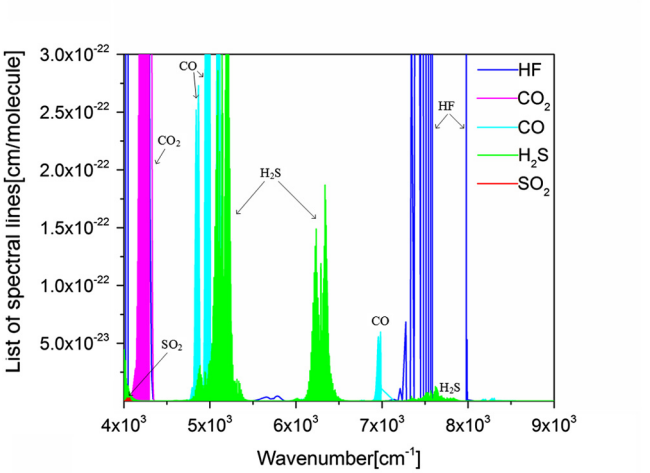


**Fig. 2** The absorption spectra of the partial decomposition of $SF_6$ in IR. All data come from HITRAN on the Web, 296 K, 1 atm.

products. We can exploit this feature to detect products using laser light sources of specific wavelengths to effectively eliminate interference from other products.

Compared with chemical detection, optical detection has many advantages such as fast response, high sensitivity, only requiring a small sample, and sample reusability. Most of the main $SF_6$ decomposition products can be detected optically. Moreover, optical detection can fulfill all requirements of gas detection devices in the power industry, including on-line monitoring and portable detection. Detection devices based on UV spectroscopy and fluorescence spectroscopy can be modularized, have a compact structure, and are portable.[22,23] Fourier transform infrared spectrometry (FTIR) and photoacoustic spectroscopy (PAS) have been used for the on-line monitoring of certain gases.[24–27] In summary, optical detection has considerable application potential for the detection of $SF_6$ decomposition products.

So far, numerous studies regarding the detection of $SF_6$ decomposition products have been conducted that have employed IR and UV spectroscopy, such as IR spectroscopy, UV fluorescence, and PAS. These studies have obtained some relevant results. However, most have focused on a specific method without providing an overview of the various optical detection methods. Therefore, herein, we comprehensively review the application of optical detection technologies for detecting $SF_6$ decomposition products according to UV and IR spectroscopy. In addition, we propose two methods that can be applied in this field.

## 2 UV Spectroscopy

### 2.1 *Differential Optical Absorption Spectroscopy*

Differential optical absorption spectroscopy (DOAS) was proposed by NOXON[28] in the early 1980s. Platt and Perner[29,30]—at the Institute of Environmental Physics, Heidelberg University, Germany—extended the technology to research on the tropospheric atmosphere. The principle of DOAS involves separating the broadband and narrowband spectral structures in an absorption spectrum to isolate the narrow target gas absorption.[31] In the absorption spectrum, the influence of Rayleigh scattering, Mie scattering, and turbulence causes very broad or smooth spectral characteristics, whereas the target gas exhibits narrowband absorption structures. In Fig. 3, the black line denotes the absorption cross section, which contains the broadband and narrowband features, whereas the red line denotes the broadband feature separated from the absorption cross section. The inset with the blue line illustrates the differential absorption

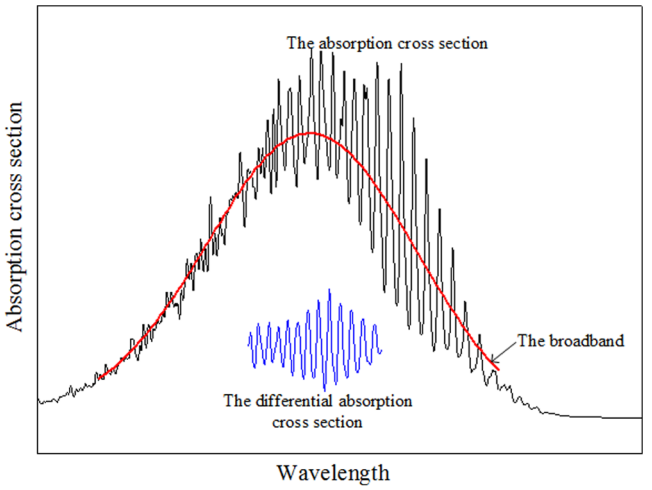


**Fig. 3** Differential spectrum schematic. The black line is the absorption cross section, which contains the broad- and narrowband; the red line is the broadband that is separated from the absorption spectrum; the blue line is the differential absorption cross section.

cross section, which only contains the absorption feature of the target gas.

In DOAS, the influence of spectral absorption caused by Rayleigh scattering and Mie scattering can be effectively eliminated, and the differential spectrum that only reflects the absorption feature of the target gas is obtained. Moreover, when electronic transitions occur in the UV region, they are accompanied by molecular vibrational and rotational energy transitions. Spectral intensity in UV spectra is several orders of magnitude higher than that in IR spectra. Therefore, this technology has high detection precision.

The decomposition products of $SF_6$ that have absorption characteristics in UV spectroscopy are mainly $SO_2$, $H_2S$, and $CS_2$. These products have been investigated in other fields, such as atmospheric chemistry and environmental engineering. The researchers in these fields have attempted to achieve high-sensitivity and portable monitoring.[32–34] Vita et al.[32] could design and construct a lightweight, portable, and low-power long-path DOAS instrument for use at remote locations, specifically to measure the degassing from active volcanic systems, due to the developments in fiber-coupling telescope technology and the availability of UV light-emitting diodes (LEDs). Their instrument could measure $SO_2$ and potentially other trace gases through long open paths around volcanic vents. The instrument's $SO_2$ detection limit was 8 ppm. Degner et al.[33] developed a set of optical sensing systems employing an LED lamp as a light source. Compared with the traditional deuterium and xenon light sources, the LED light source is cheaper, longer lasting, more stable, and more suitable for local and on-line monitoring. The detection limits of $SO_2$ and $NO_2$ were 1 ppm, and the detection limit of $O_3$ reached 30 parts per billion (ppb). Nasse et al.[34] used a laser-driven light source instead of the traditional Xe arc lamp and an optical fiber bundle in the telescope for the transmission and reception of the measurement signal to obtain autonomous long-term trace gas measurements. These improvements enhanced the wavelength-selective coupling from the light source into the fiber, which reduced stray light. Moreover, the coupling and configuration of the optical fiber was optimized compared with previous designs to maximize light throughput and reduce stray light.

The open paths have been used to increase the optical length in the applications.[32–34] However, these applications are unsuitable for detecting the decomposition products of $SF_6$. The $SF_6$-insulated electrical equipment is enclosed. A suitable option for detecting gas in the equipment involves introducing the gas into a gas cell, which is integrated into the portable device. Zhang et al.[35] reported a UV-DOAS device for detecting $SF_6$ decomposition products with a portable design, and the schematic diagram is shown in Fig. 4. The device mainly comprised a light source, gas cell, spectrometer, and laptop. The differential absorption spectrum of $SO_2$ was obtained by performing Sym14 wavelet-layering treatment. The $SO_2$ concentration was calculated according to the characteristic peak obtained through fast Fourier transformation in the 190- to 230-nm and 290- to 310-nm bands. The results showed that the device had a lower detection limit in the 190- to 230-nm band than in the 290- to 310-nm band, and the detection limit was 132.4 ppb with signal-to-noise ratio $(\mathrm{SNR}) = 3$.

Zhang et al.[36] also investigated the quantitative detection of $CS_2$ using this device. The detection limit is 8.65 ppb in the 190- to 210-nm band. However, Fig. 2 shows that an absorption spectrum of $SO_2$ continues to exist in this band. To avoid interference of this product, the absorption spectrum of the 290- to 310-nm band can be used to detect the $SO_2$ concentration initially. Then, the interference of $SO_2$ can be deducted to obtain the exact concentration of $CS_2$ in the 190- to 210-nm band, as shown in Fig. 5.

Few studies have been conducted on the detection of $H_2S$ based on UV-DOAS. Zhang et al.[37] established the relationship between the concentration of $H_2S$ and its UV absorption spectrum using wavelet transform and frequency-domain analysis. In addition, they studied in detail the overlap of $H_2S$ and $CS_2$ in the 190- to 210-nm band. $H_2S$ absorption in the wave number domain was discovered to be affected by $CS_2$ and cannot be quantitatively analyzed directly by inversion. However, $CS_2$ absorption in the wave number domain remains unaffected, which means that $CS_2$ concentration can be determined, as shown in Fig. 6. The influence of $CS_2$ on $H_2S$ was determined experimentally to confirm the corrected inversion formula, and thus, quantitative measurement of mixed $CS_2$ and $H_2S$ gas was realized.

Through multiple studies on portable detection devices for $SF_6$ decomposition products, Zhang et al. quantitatively detected $SO_2$, $H_2S$, and $CS_2$ in the $SF_6$-insulated electrical equipment. The detection device is low cost, with simple structure, and reliable sensitivity, which makes it suitable for applications in the power industry.

### 2.2 *UV Fluorescence Method*

The UV fluorescence method is a gas quantification method based on detection of the intensity of the fluorescence spectrum emitted by a gas molecule returning to its ground state from an excited state. After a molecule absorbs excitation light of a certain wavelength, it returns to its lowest excited energy level through vibration relaxation and subsequently transitions downward to generate fluorescence.[38] The wavelength of the fluorescence is generally longer than that of the excitation light. Fluorescence can be measured with a very low background signal so long as the excitation light is

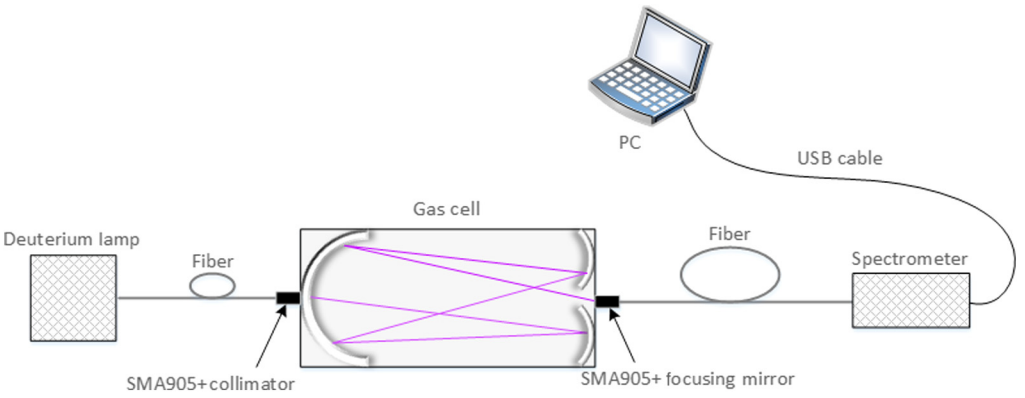


**Fig. 4** The schematic diagram of the UV-DOAS detection system.

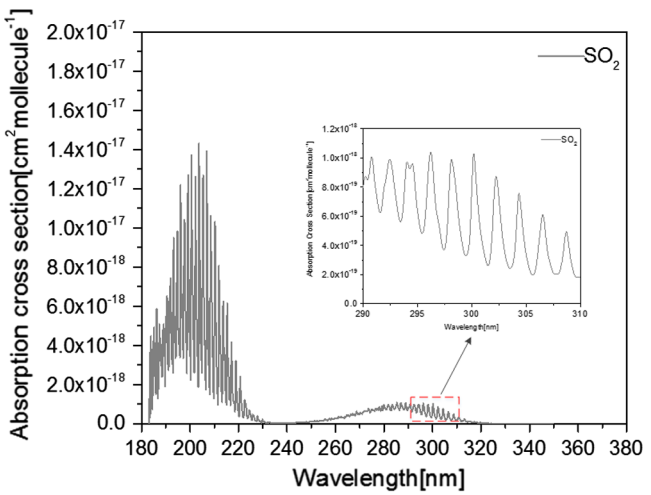


**Fig. 5** The absorption spectrum of $SO_2$ in 190 to 310 nm.

shunted by effective measures. The intensity of the fluorescence signal, $I_f$, is proportional to the intensity of the light absorbed by the molecule:

$$I_f = \psi(I_0 - I), \tag{1}$$

where $I_0$ is the input light intensity, $I$ is the output light intensity, and $\Psi$ is a constant that is determined using the fluorescence quantum efficiency.

According to the Lambert–Beer law, the relationship between $I_f$ and the medium concentration can be established as follows:

$$\begin{aligned} I_f &= \psi I_0(1 - 10^{-\varepsilon lc}) \\ &= \psi I_0\left[2.3\varepsilon lc - \cdots \frac{(-2.3\varepsilon lc)^n}{n!} - \cdots\right] \\ &= 2.3\psi\varepsilon lc I_0(\varepsilon lc < 0.05), \end{aligned} \tag{2}$$

where $c$ is the medium concentration, $\varepsilon$ is the gas molecule molar absorption coefficient, and $\varepsilon lc$ is absorbance.

When $I_0$ is constant, Eq. (2) can be expressed as

$$I_f = Kc. \tag{3}$$

The gas concentration can be quantified by measuring the fluorescence intensity. UV fluorescence spectroscopy is more sensitive than UV-DOAS because it measures the fluorescence intensity superimposed on a very small background and it has favorable selectivity. However, not all substances fluoresce under certain conditions, indicating that the application range of UV fluorescence spectroscopy is narrower than that of UV-DOAS.

Among the decomposition products of $SF_6$, $SO_2$ has been the focus of many UV fluorescence detection studies. Pulsed fluorescence monitoring of $SO_2$ based on the UV fluorescence principle has become the standard method in many

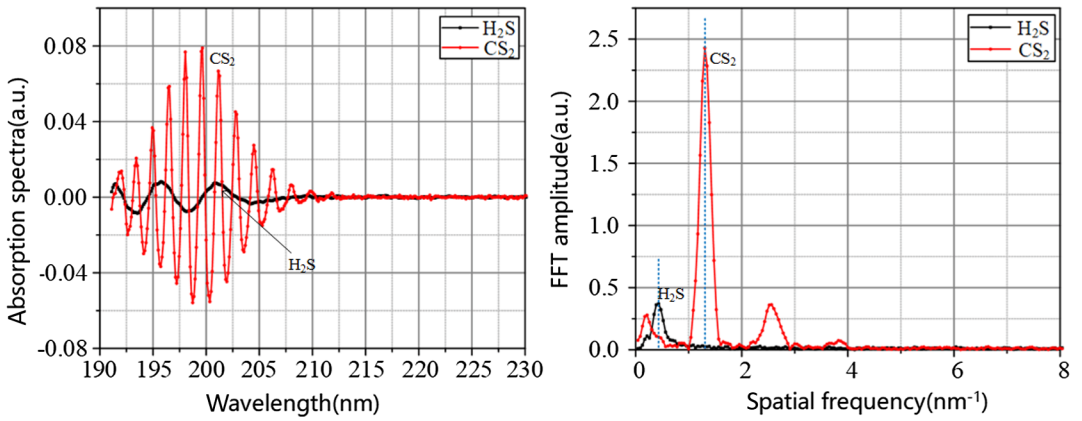


**Fig. 6** Wavenumber-domain curves of $CS_2$ and $H_2S$. The absorption of $CS_2$ in the wave number domain will not be affected, its concentration can be determined.

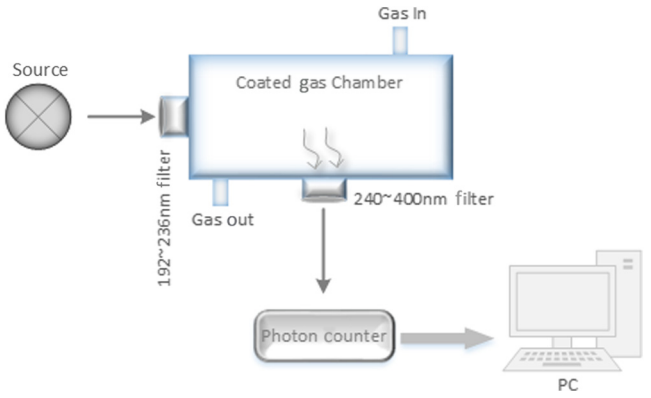


**Fig. 7** The structure of UV fluorescence detection device.

countries, for the World Health Organization, and in global testing systems. UV fluorescence detection devices for $SO_2$, such as Model T100 (Teledyne-API), 43*i*-TLE (Thermo Electron Corporation), and SERINUS 50 (Ecotech), have been commercialized and mainly used for environmental monitoring. These devices can achieve a detection limit of the order of ppb. However, UV fluorescence detection devices are relatively expensive. Moreover, the background gas in the $SF_6$-insulated electrical equipment is different from that in air monitoring. Zhou et al.[39] reported a UV fluorescence detection device for $SF_6$ decomposition products, as shown in Fig. 7. A deep-UV deuterium lamp with an output range of 190– to 00 nm was used as the light source. The input to the gas cell was supplied through a filter with a range of 192 to 236 nm. Fluorescence detection was performed at 90 deg with respect to the excitation beam to avoid the strong radiation of the excitation light. At the output, a filter with a range of 240 to 400 nm was employed to exclude scattering interference from the excitation light. A photomultiplier tube is used for detection. The entire device was placed in a self-designed dark box to reduce external interference. The inside of the gas cell was coated with Teflon, and the connector was made of stainless steel and Teflon tubing to prevent $SO_2$ adsorption. The detection limit of the device was 110.94 ppb with SNR = 3 in the background gas of $SF_6$. The background signals were not affected by changes of temperature and pressure, whereas the $SO_2$ fluorescence signals show a strong growth trend with the increase of temperature and pressure.

The structure of this device is simple and compact. The optical path of the gas chamber is 0.2 m, and its volume is 360 mL. The commercial light source and detector are miniaturized and integrated. Therefore, a portable or handheld device can be developed on the basis of this structural scheme.

## 3 Infrared Spectroscopy

### 3.1 *Fourier Transform Infrared Spectrometry*

An FTIR spectrometer is a preferred research instrument due to the high SNR, high resolution, accurate wavelength, favorable repeatability, and stability provided by it.[40] FTIR has numerous applications in many fields. The detection of $SF_6$ decomposition products using FTIR technology can be traced back to the 1990s. Piemontesi et al.[41] studied the effect of $H_2O$ and $O_2$ on the decomposition products of $SF_6$ using FTIR. They detected the products $S_2F_{10}$, $SOF_2$, $SOF_4$, $CF_4$, HF, and CO and discovered that the presence of $H_2O$ and $O_2$ helped reduce the $S_2F_{10}$ content. Pilzecker et al.[42] analyzed the characteristics of the colorimetric tube, ion mobility spectrometry, and FTIR in studying the decomposition products of $SF_6$. Ion mobility spectrometry and FTIR showed strong correlation in $SOF_2$ detection. The detection limit of ion mobility spectrometry was found to be 40 ppm. Compared with the other two methods, the colorimetric tube had a lower detection limit and had difficulty detecting $SO_2$ and HF. Ding et al.[43] used FTIR to analyze the adsorption of $SF_6$ and its decomposition products by employing carbon nanotube sensors, and they proposed a new method for detecting $SF_6$ decomposition products. IEC60480[44] specifies the test standard for the detection of $SF_6$ decomposition products using FTIR.

Zhang et al.[45–50] conducted a series of FTIR studies on the decomposition products of $SF_6$. The studies were based on the principle of White-Cell. They designed a gas cell with a 20-m-long path length, which was matched with FTIR. By comparing the results obtained using the FTIR equipped with this gas cell with those obtained using GC, the FTIR was found to detect a greater number of products than the gas chromatograph. The typical wave numbers of the absorption of $SF_6$ and its decomposition products in the IR band were obtained, as listed in Table 2. In addition, Zhang et al. used two-dimensional correlation spectroscopy to magnify the spectrum so that $SF_6$ decomposition products such as $SOF_2$, $SO_2F_2$, $SF_4$, $SOF_4$, CO, $SO_2$, and $CF_4$ could be detected under the background of $SF_6$, which successfully solved a problem: that the information of other products is submerged owing to the strong absorption peak of $SF_6$. Zhang et al. conducted numerous studies on the mechanism of $SF_6$ decomposition under different discharge conditions, including changes in the types of decomposition products and in the gas production rates of different products. They made important contributions to the theory, which is based on $SF_6$ decomposition product analysis to determine insulation faults in equipment.

Although FTIR can be used for on-line monitoring,[24,25] there exists no commercial FTIR spectrometer for the on-line monitoring of $SF_6$ decomposition products. The gas

**Table 2** Typical absorption peaks of $SF_6$ decomposition products.

| Type | Wavenumber ($cm^{-1}$) | Wavelength ($\mu m$) |
|---|---|---|
| $SO_2F_2$ | 539/544/552 | 18.6/18.4/18.1 |
| $SOF_2$ | 530/1330/1340 | 18.9/7.52/7.46 |
| $CF_4$ | 1283 | 7.79 |
| $SO_2$ | 1169/1360 | 8.55/7.35 |
| $H_2S$ | 2625 | 3.81 |
| HF | 3644 | 2.74 |
| $SF_4$ | 746 | 13.4 |
| $SOF_4$ | 752 | 13.3 |
| $SF_6$ | 610/946/1270/1595/1720 | 16.4/10.6/7.9/6.27/5.81 |

cell and quantitative algorithm must be customized if FTIR has to be used for on-line monitoring. FTIR is primarily used in the laboratory for analysis. With the long-path gas cell, detecting almost all the $SF_6$ decomposition products is possible. The usual practice involves performing a preliminary detection of the products in the equipment through the portable or on-line detection device. If abnormal gases are found, the internal gas of the equipment can be sampled. Detailed analysis can be then performed in the laboratory using FTIR.

### 3.2 *Photoacoustic Spectroscopy*

PAS is an indirect spectroscopic method that combines the theory of IR absorption spectroscopy with the photoacoustic (PA) effect. The concentration of a gas can be calculated by measuring the intensity of the acoustic signal excited by the PA effect. When the excited electrons return to the ground state, energy is released outward in two ways: radiation and nonradiative transitions, where the nonradiative transition releases heat and changes the ambient pressure. If the incident light is modulated and injected into the gas cell at a certain frequency, a periodic heat source is formed that changes the pressure periodically, resulting in the generation of an acoustic signal. The gas concentration can be calculated indirectly by detecting the acoustic signal. This is the basic principle of PAS, as shown in Fig. 8.

PAS has many advantages over traditional absorption spectroscopy:

1. The strength of PA signals is related to the light energy absorbed by gas molecules. If there is no absorption, there is no PA signal, so it is a background-less technology.
2. The light intensity detector in traditional absorption spectroscopes is wavelength-dependent, whereas the detector used in a PAS is wavelength-independent.
3. PAS offers good stability and high sensitivity. By using a laser light source and high-sensitivity microphones, theoretical detection limits of the order of ppb can be achieved;[51,52]
4. PAS detection system is smaller, has fast response, and is easy to monitor on site.

Based on these advantages, PAS has received widespread attention. A few studies have reviewed the research on the use of PAS for gas detection. Elia et al.[53] introduced PAS gas-sensing technology based on semiconductor laser sources. An IR tunable semiconductor laser was considered an ideal light source for gas detection, and it has been used widely in environmental monitoring, chemical detection, industrial emission monitoring, and other fields. In addition, the standard PAS and differential PAS methods were summarized, and quartz-enhanced PAS was discussed. Pogány[54] introduced the development of PAS and discussed the special problems associated with PAS in practical applications, including the problems of noise and spectral interference. Pogány summarized the practical applications of PAS, including in environmental monitoring and industrial fields, and outlined prospects for the development of PAS. Miklos[55] described three types of PA cells used in PAS—the one-dimensional acoustic resonator [Figs. 9(a) and 9(b)], Helmholtz resonator [Figs. 9(c)], and cavity resonator [Figs. 9(d)–9(f)]—and discussed their application in gas detection.

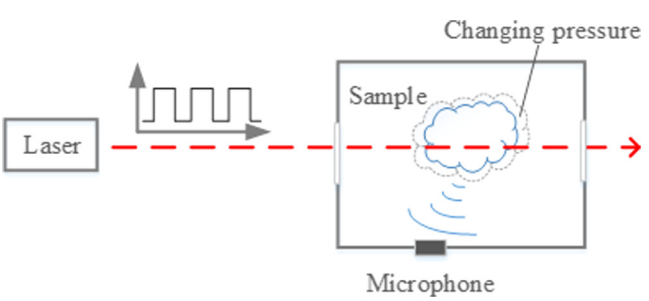


**Fig. 8** The principle of PAS.

PAS can be used to detect $SF_6$ decomposition products with absorption characteristics in the IR region. Lin et al.[56] developed a PAS device for detecting $SF_6$ decomposition products, as shown in Fig. 10. The device employed broadband IR light as the light source, a highly sensitive electret microphone for sound signal detection, and a mechanical chopper for light modulation, and the device could detect $SO_2F_2$, $SO_2$, $CF_4$, and $CO_2$ with detection precision of 0.831, 1.888, 2.213, and 5.695 $\mu$V/ppm, respectively. Qiu et al.[57] used a broadband IR source with a wavelength of 0.6 to 25 $\mu$m to obtain a PAS device for detecting $SOF_2$. A chopper was employed for modulation. To avoid the influence of the absorption of other products, a filter with a range of $7440 \pm 20$ nm was used. The longitudinal resonant PA cell was made of pure copper, and both ends were sealed with ZnSe. The measured quality factor of the cell was 47. The detection limit of the device was 4.6 ppm, and the average error was 5.9%. According to Qiu et al., PAS is a reliable method for the on-line monitoring of $SF_6$-insulated electrical equipment.

The performance of PAS can be further enhanced by improving their components. Wu et al.[58] used a customized quartz tuning fork as a microphone and amplified light power using an erbium-doped fiber amplifier. They developed a PAS sensor for detecting $H_2S$, and the detection limit of this sensor was 890 ppb. Varga et al.[59] developed a two-channel $H_2S$ on-line monitoring system with a detection limit of 0.5 ppm, which was suitable for the natural gas industry. Laboratory and field tests showed that this system could perform long-term and stable monitoring in harsh industrial environments.

The use of an interferometric cantilever sensor instead of a conventional microphone can enhance the sensitivity by at least one order of magnitude.[60] Gasera Ltd. had developed various PA detectors based on the interferometric cantilever.[61,62] The working principle of the cantilever-enhanced PA cell is shown in Fig. 11. Interaction between the gas in the cell and the modulating light leads to changes in pressure. The changing pressure causes the cantilever to vibrate. A Michelson interferometer is employed to optically measure the displacement of the free end of the cantilever and thus acquire a PA signal.

Zhang et al.[63] analyzed the decomposition of $SF_6$ and its reaction with other impurities to form $H_2S$ using Materials Studio. They then employed a cantilever-enhanced PAS to detect $H_2S$. The PA cell and microsilicon cantilever microphone system were manufactured by Gasera Ltd. A distributed feedback laser diode with a center wavelength of

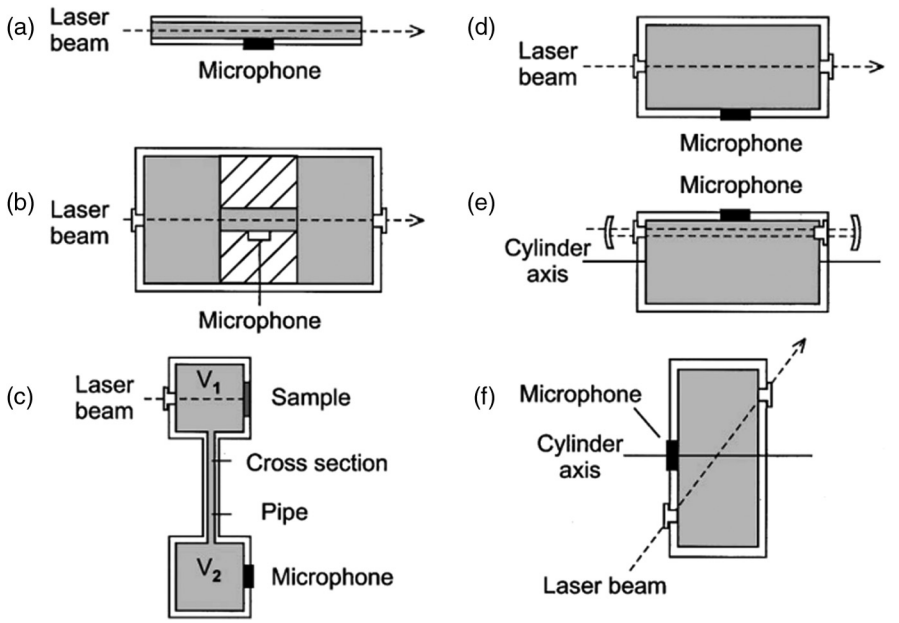


**Fig. 9** Different types of PA cells. The figure comes from Miklos.[55] The (a, b) one-dimensional acoustic resonator, (c) the Helmholtz resonator, and (d–f) the cavity resonator.

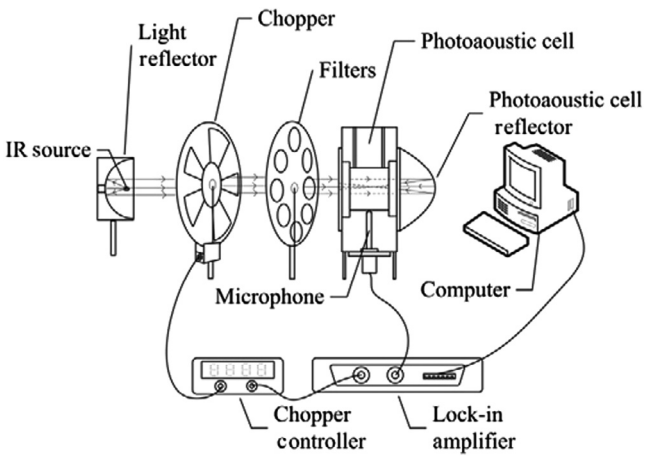


**Fig. 10** The structure of PAS device. The figure reproduced from Ref. 56.

1577.86 nm was adopted in the study. The results show that under two background gases, $N_2$ and $SF_6$, the detection limit was 0.84 and 1.75 ppm, respectively. Zhang et al.[63] analyzed the factors that influence cantilever-enhanced PAS gas detection and found that the change in the PA signal amplitude decreases with an increase in the pressure or temperature of the PA cell. They also found that the detection platform is more sensitive to pressure than temperature.

The on-line monitoring PAS system has a few commercial applications. It has promising applications for $SF_6$-insulated electrical equipment. After the target gas and corresponding light source are determined, an on-line monitoring device with a PA cell can be developed for $SF_6$ decomposition products. A feasible scheme of on-line monitoring PAS for $SF_6$-insulated equipment is shown in Fig. 12. Because the pressure in the equipment is several times higher than atmospheric pressure, a pressure reducing valve is installed in

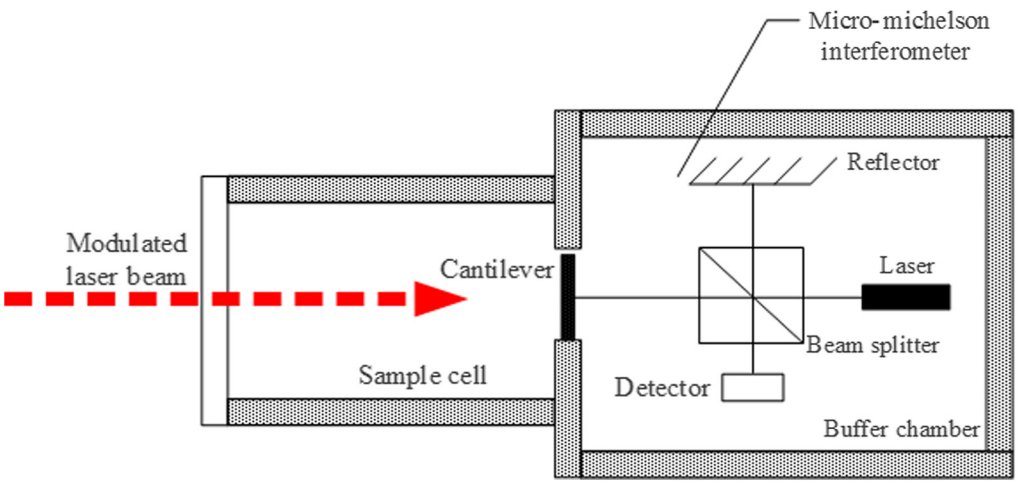


**Fig. 11** The principle of the cantilever-enhanced PA cell. Sample cell and micro-Michelson interferometer.

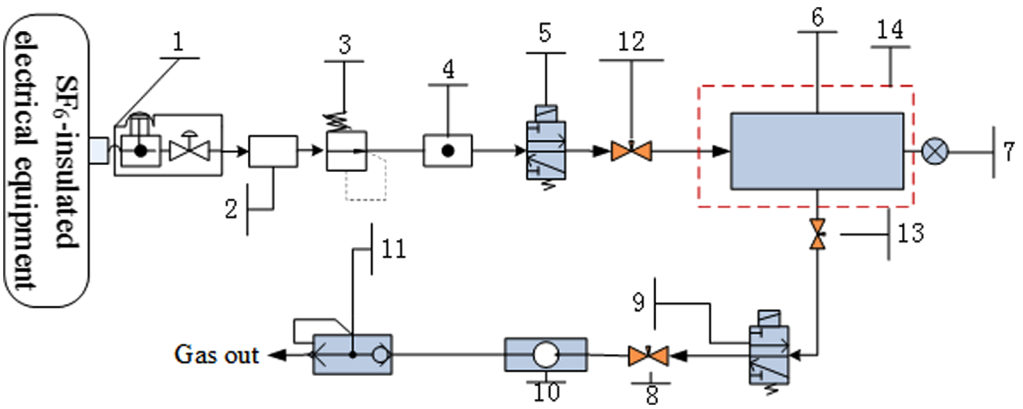


**Fig. 12** The schematic diagram of on-line monitoring PAS for the $SF_6$-insulated electrical equipment. (1) Sampling port, (2) metal dust filter, (3) pressure reducing valve, (4) three-way valve, (5) switch valve, (6) PAS device, (7) pressure sensor, (8) restriction valve, (9) switch valve, (10) vacuum pump, (11) check valve, (12, 13) flow control valve, and (14) passive vibration isolation device.

the gas path. A three-way valve is used to introduce pure and dry $N_2$ to clean the PA cell.

## 4 Technology for Detecting SF6 Decomposition Products

With the development of optical detection technology, researchers are pursuing higher detection accuracy, higher sensitivity, and faster detection time. Equally, it is hoped that the structure would be as simple and compact as possible for onsite or on-line monitoring. Thus, many optical technologies are continuing to emerge. The following are two technologies that can be used for detecting $SF_6$ decomposition products.

### 4.1 *Cavity Ring-Down Spectroscopy*

CRDS is a direct absorption technique that can be performed with pulsed or continuous light sources. A significantly higher sensitivity can be obtained with CRDS than with conventional absorption spectroscopy. CRDS was formally proposed by O'Keefe and Deacon in 1988.[64] CRDS uses the ring-down time to invert the gas concentration, which reduces the impact of light source fluctuation on the detection results. In addition, light can be reflected back and forth multiple times in the ring-down cavity, which can extremely improve the gas absorption path.

Pulse CRDS (P-CRDS) is used as an example. Its working principle is shown in Fig. 13. The detection system consists of a pulsed laser source, a ring-down cavity composed of two high-reflectance mirrors (>99.9% reflectance), a photodetector, and other products. The pulsed laser is coupled with the ring-down cavity, and light is reflected multiple times in the ring-down cavity. During each reflection, the laser interacts with the target gas while some weak light is transmitted. According to the Lambert–Beer law, the transmitted light signal decays exponentially. The ring-down time $\tau$ is the time required for the light intensity to decay to $1/e$ of the initial light intensity. The change in the ring-down time $\tau$ reflects the system loss, including intrinsic losses and gas absorption losses. The intrinsic system losses, such as connector loss and fiber loss, are constant. Therefore, the gas absorption loss can be determined by the change in the ring-down time $\tau$, and then, the gas concentration can be calculated. For example, when the ring-down time decreases, the gas absorption loss increases and the gas concentration thus increases.

CRDS has strong anti-interference ability and high detection accuracy, and it is suitable for trace gas detection. Several scholars have used it to detect $SF_6$ decomposition products. Zhang et al.[65] adopted a modular design method based on CRDS to design an on-line system for monitoring $SF_6$ decomposition products, and the feasibility of this system for detecting $SF_6$ decomposition products was demonstrated.

However, the limitation of CRDS lies in its dependence on ultrahigh-reflectivity mirrors. In actual measurements, if the mirror reflectance decreases owing to mirror pollution or ring-down cavity vibration, the measurement error is dramatically increased. Furthermore, pattern matching of the cavity is a problem. To solve these problems, a new type of CRDS technology is introduced herein: fiber loop ring-down spectroscopy (FLRDS).[66–69]

FLRDS is based on CRDS. An optical fiber is used to replace the ring-down cavity, and this fiber directs the pulsed light to circulate in the fiber loop. The basic principle of FLRDS is shown in Fig. 14. The equipment is composed of two $2 \times 1$ couplers and a gas cell. Pulsed light enters the fiber ring cavity through coupler C1 to circulate, and during each cycle, the light interacts with the gas in the cell. A small percentage of the light enters the photodetector through coupler C2, but most of the light continues to circulate in the fiber ring cavity, and this continues until the light is completely attenuated.

All-fiber connections are employed in FLRDS. Forming a fiber sensor network for the on-line monitoring of trace gas is easy.[70] However, the detection precision of FLRDS cannot currently meet the requirement of $SF_6$ decomposition products.[68,71,72] Thus, further detailed research is required.

### 4.2 *Photonic Crystal Fibers*

A PCF, also called a microstructured fiber, is shown in Fig. 15. The interior of such a fiber can be an air-core structure that allows for the transmission of photons within the air core.[73] This enhances the interaction of light and air, resulting in higher excitation efficiency and smaller losses. It is possible to create cells with long absorption paths.

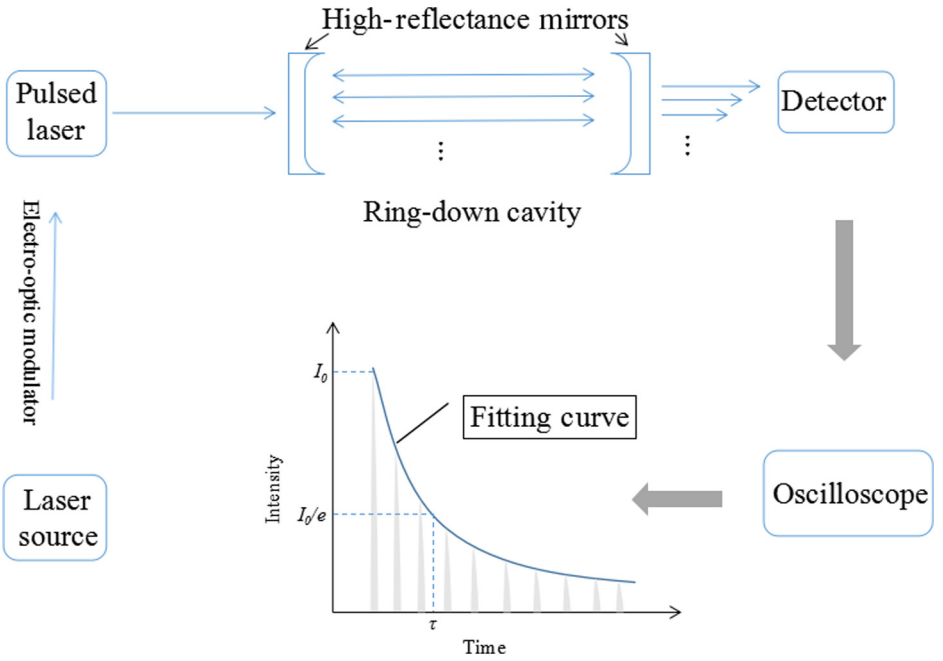


**Fig. 13** The principle of CRDS.

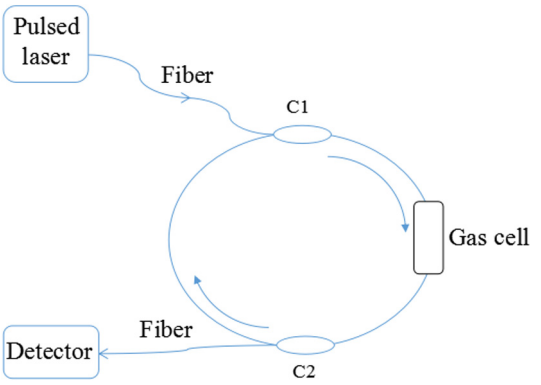


**Fig. 14** The basic principle of FLRDS.

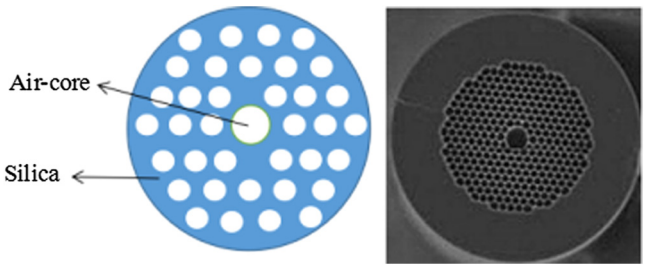


**Fig. 15** The structure of PCF.

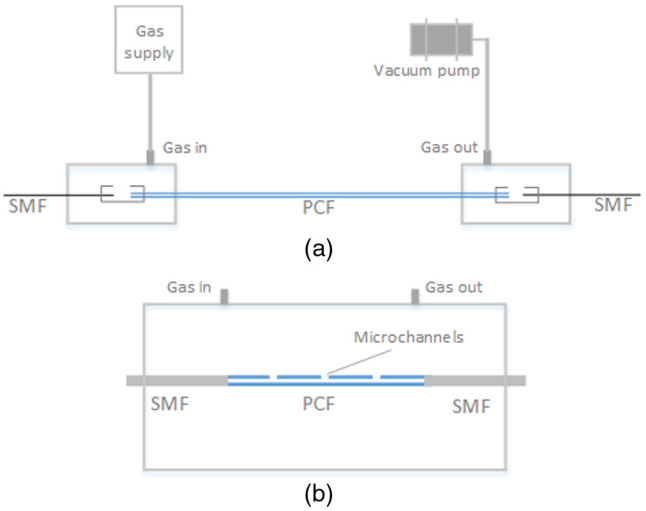


**Fig. 16** Two ways to make the gas enter into the cell. (a) Using microgap and (b) drilling microchannels.

However, it is necessary to consider how to input the gas into the cell. There are generally two ways to achieve this: to create a small gap between the PCF and the input/output of the optical fiber to allow gas to flow in; and to use a femtosecond laser to drill holes in the side of the PCF, which enables accelerated inflow of gas, as shown in Fig. 16.

Li et al.[74] chose to create a gap of 10 $\mu$m between the PCF and the input/output of the fibers. They evacuated the gap for 12 h after cleaning it with $N_2$. Then, the target gas flowed into the PCF cell under a pressure of 100 kpa. The results showed that the transmission loss of $CH_4$ at concentrations of 0.5% to 4% tended to stabilize after 6 min; the transmission fluctuation for $C_2H_6$ with 10% concentration was 0.2 dB in the first 2000 s. Jin et al.[75] used a femtosecond laser to drill the side of a 0.62-m-long PCF, and the total loss after drilling was 4 dB. In addition, they used an all-fiber photothermal spectroscope with the PCF to detect $C_2H_2$, obtaining a detection limit of 30 ppb. Lehmann et al.[76] indicated the characteristics of different modes of gas diffusion: a PCF microgap required the use of a vacuum pump or pressurization to inject gas, and the gas diffusion time was longer. Moreover, fabricating the PCF cell by means of femtosecond laser side-drilling was complicated,

**Table 3** Several optical detection methods for $SF_6$ decomposition products.

| Method | Types | | | | | | Application | Cost | Sensitivity | Speed |
|---|---|---|---|---|---|---|---|---|---|---|
| | $SO_2$ | $H_2S$ | $CS_2$ | $SOF_2$ | $SO_2F_2$ | $CF_4$ | | | | |
| UV-DOAS | √ | √ | √ | | | | Portable | Medium | Sub-ppm | Fast |
| UV fluorescence | √ | | | | | | Portable or handheld | Low | Sub-ppm | Fast |
| FTIR (with 20 m gas cell) | √ | √ | | √ | √ | √ | Laboratory or on-line monitoring | High | ppm | Medium |
| PAS | √ | √ | | √ | √ | √ | On-line monitoring | High | Sub-ppm | Fast |

and there was a risk of destroying the PCF structure during the drilling process.

Gas detection with PCFs has extremely high precision. However, the production process of the gas cell is complicated. The gas cell may achieve popularity for commercial applications in the future. Thus, we can continue to pay attention to the developments in this field.

## 5 Conclusion

The various advantages of the optical detection method, such as high precision and speed, portability, on-line monitoring, and nondestructive measurement, enable it to have good application prospects in the power industry. Different methods have different application scenarios, and their cost, detection technique, and sensitivity also vary. Table 3 summarizes the detection methods mentioned herein. Because CRDS and PCF have few applications in the detection of $SF_6$ decomposition products, they are not listed in the table.

The detection devices based on UV-DOAS and UV fluorescence can conveniently sample and detect $SF_6$ decomposition products on-site. The UV fluorescence device can also be modified into a handheld device, which can reduce the work intensity of on-site inspection personnel. The detection devices based on UV-DOAS and UV fluorescence have a fast response. Moreover, the cost of the UV-DOAS and UV fluorescence devices is lower than that of FTIR and PAS. However, few products can be detected with the UV-DOAS and UV fluorescence devices. FTIR can be used to detect almost all products. Although it can be used for on-line monitoring, the operation process for multiproduct measurement is complicated. The operators must be trained accordingly. Its response speed is related to the spectral resolution. A long time is required to perform a fine-resolution analysis. Therefore, analyzing the sample gas in the laboratory through FTIR is the most suitable option. PAS, the most suitable method for on-line monitoring, can be used to detect multiple products with a corresponding light source or filter. However, PAS is costlier than the UV-DOAS and UV fluorescence devices.

In summary, for the consumer and junction substations, on-line monitoring PAS can be used to ensure real-time access to the insulation. The UV-DOAS and UV fluorescence devices are cheap and easy to use. These devices can be used in the routine maintenance of equipment. The UV-DOAS and UV fluorescence devices can detect limited components. However, when an abnormal gas is detected, it can be removed from the equipment for FTIR detection to quantitatively analyze the products in detail. By combining various optical detection methods, the detection accuracy of $SF_6$ decomposition products can be ensured. Thus, the types and severity of insulation defects can be determined in an effective and a timely manner.

### Acknowledgments

This work was supported by Key Program of National Natural Science Foundation of China (51537009).

### References

1. R. J. Van Brunt and J. T. Herron, "Fundamental processes of $SF_6$ decomposition and oxidation in glow and corona discharges," *IEEE Trans. Electr. Insul.* **25**(1), 75–94 (1990).
2. F. Y. Chu, "$SF_6$ decomposition in gas-insulated equipment," *IEEE Trans. Electr. Insul.* **EI-21**(5), 693–725 (1986).
3. B. Belmadani, J. Casanovas, and A. M. Casanovas, "$SF_6$ decomposition under power arcs. II. Chemical aspects," *IEEE Trans. Electr. Insul.* **26**(6), 1177–1182 (1991).
4. A. Derdouri et al., "Spark decomposition of $SF_6/H_2O$ mixtures," *IEEE Trans. Electr. Insul.* **24**(6), 1147–1157 (1990).
5. C. Beyer, H. Jenett, and D. Klockow, "Influence of reactive SFX gases on electrode surfaces after electrical discharges under $SF_6$ atmosphere," *IEEE Trans. Dielectr. Electr. Insul.* **7**(2), 234–240 (2000).
6. J. M. Braun, F. Y. Chu, and R. Seethapathy, "Characterization of GIS spacers exposed to $SF_6$ decomposition products," *IEEE Trans. Electr. Insul.* **EI-22**(2), 187–193 (1987).
7. J. Tang et al., "Partial discharge recognition through an analysis of $SF_6$ decomposition products part 1: decomposition characteristics of $SF_6$ under four different partial discharges," *IEEE Trans. Dielectr. Electr. Insul.* **19**(1), 29–36 (2012).
8. J. Tang et al., "Partial discharge recognition through an analysis of $SF_6$ decomposition products part 2: feature extraction and decision tree-based pattern recognition," *IEEE Trans. Dielectr. Electr. Insul.* **19**(1), 37–44 (2012).
9. S. Tominaga et al., "$SF_6$ gas analysis technique and its application for evaluation of internal conditions in $SF_6$ gas equipment," *IEEE Trans. Power Appar. Syst.* **PAS-100**(9), 4196–4206 (1981).
10. J. M. Braun and F. Y. Chu, "Novel low-cost $SF_6$ arcing byproduct detectors for field use in gas-insulated switchgear," *IEEE Trans. Power Delivery* **1**(2), 81–86 (1986).
11. J. K. Wittle et al., "Fault-detection sensors for gas insulated equipment," NASA STI/Recon Technical Report N, 83 (1982).
12. S. Okabe et al., "Detecting characteristics of $SF_6$ decomposed gas sensor for insulation diagnosis on gas insulated switchgears," *IEEE Trans. Dielectr. Electr. Insul.* **15**(1), 251–258 (2008).
13. F. Y. Chu, "Gas analysis as a diagnostic tool for gas-insulated equipment," in *Gaseous Dielectrics V*, L. G. Christophorou and D. Bouldin, Eds., pp. 462–471, Pergamon Press, New York (1987).
14. H. Wang et al., "Detection of ppb level $SO_2$ in $H_2$ by an adsorption–desorption gas chromatography method," *Int. J. Hydrogen Energy* **35**(7), 2994–2996 (2010).
15. H. Chang et al., "Microfabricated gas chromatograph for sub-ppb determinations of TCE in vapor intrusion investigations," *Proc. Eng.* **5**(6), 973–976 (2010).
16. Z. Pegram, M. T. Kwasniewski, and G. L. Sacks, "Simplified method for free $SO_2$ measurement using gas detection tubes," *Am. J. Enol. Vitic.* **64**(3), 405–410 (2013).
17. X. Zhang et al., "Mechanism and application of carbon nanotube sensors in $SF_6$ decomposed production detection: a review," *Nanoscale Res. Lett.* **12**(1), 177 (2017).

18. X. Zhang, Y. Gui, and X. Dong, "Preparation and application of $TiO_2$ nanotube array gas sensor for $SF_6$-insulated equipment detection: a review," *Nanoscale Res. Lett.* **11**(1), 302 (2016).
19. X. Zhang, "Experimental study of carbon nanotubes gas sensor detecting $SF_6$ partial discharge decomposition components," *Trans. China Electrotechn. Soc.* **26**(11), 121–126 (2011).
20. X.-X. Zhang et al., "DFT calculations on the adsorption of component $SF_6$ decomposed under partial discharge onto carbon nanotubes modified by -OHoh," *Acta Phys. Sin.* **61**(15), 415–418 (2012).
21. J. Suehiro, G. Zhou, and M. Hara, "Detection of partial discharge in $SF_6$ gas using a carbon nanotube-based gas sensor," *Sens. Actuators B* **105**(2), 164–169 (2005).
22. S. Camou et al., "PPB-level detection of benzene diluted in water by bubbling extraction system and UV spectroscopy based measurements," in *TRANSDUCERS Int. Solid-State Sensors, Actuators and Microsystems Conf.*, IEEE, pp. 261–264 (2007).
23. K. Davitt et al., "290 and 340 nm UV LED arrays for fluorescence detection from single airborne particles," *Opt. Express* **13**(23), 9548–55 (2005).
24. K. Kortenbruck et al., "Determination of the diffusion coefficient of $CO_2$, in the ionic liquid EMIM NTf 2 using online FTIR measurements," *J. Chem. Thermodyn.* **47**(12), 76–80 (2012).
25. A. Sánchez, E. Eddings, and F. Mondragón, "Fourier transform infrared (FTIR) online monitoring of NO, $N_2O$, and $CO_2$ during oxygen-enriched combustion of carbonaceous materials," *Energy Fuels* **24**(9), 4849–4853 (2010).
26. F. J. M. Harren et al., "Photoacoustic spectroscopy in trace gas monitoring," in *Encyclopedia of Analytical Chemistry*, R. A. Meyers, Ed., pp. 2203–2226, John Wiley & Sons, Ltd., Chichester, England (2000).
27. M. W. Sigrist, "Trace gas monitoring by laser photoacoustic spectroscopy and related techniques (plenary)," *Rev. Sci. Instrum.* **74**(1), 486–490 (2003).
28. J. F. Noxon, "Nitrogen dioxide in the stratosphere and troposphere measured by ground-based absorption spectroscopy," *Science* **189**(4202), 547–549 (1975).
29. U. Platt, D. Perner, and H. W. Pätz, "Simultaneous measurement of atmospheric $CH_2O$, $O_3$, and $NO_2$ by differential optical absorption," *J. Geophys. Res.* **84**(C10), 6329–6335 (1979).
30. U. Platt and D. Perner, "Direct measurements of atmospheric $CH_2O$, $HNO_2$, $O_3$, $NO_2$, $SO_2$ by differential optical absorption in the near UV," *J. Geophys. Res.* **85**(C12), 7453–7458 (1980).
31. U. Platt and J. Stutz, *Differential Optical Absorption Spectroscopy (DOAS)—Principles and Applications*, p. 15, Springer, Berlin (2008).
32. F. Vita, C. Kern, and S. Inguaggiato, "Development of a portable active long-path differential optical absorption spectroscopy system for volcanic gas measurements," *J. Sens. Sens. Syst.* **3**(2), 355–367 (2014).
33. M. Degner et al., "High resolution led-spectroscopy for sensor application in harsh environment," in *Instrumentation and Measurement Technology Conf.*, IEEE, pp. 1382–1386 (2010).
34. J. M. Nasse et al., "Autonomous long-term trace gas measurements using long-path differential optical absorption spectroscopy," in *EGU General Assembly Conf.*, EGU General Assembly Conference Abstracts (2017).
35. H. Zhou et al., "Quantum detection of trace sulfur dioxide based on ultraviolet differential optical absorption spectrometry," *Proc. CSEE* **37**(19), 5812–5820 (2017).
36. X. Zhang et al., "Ultraviolet differential optical absorption spectrometry: quantitative analysis of the $CS_2$ produced by $SF_6$ decomposition," *Meas. Sci. Technol.* **28**(11), 115102 (2017).
37. X. Zhang et al., "Quantitative detection of $H_2S$ and $CS_2$ mixed gases based on UV absorption spectrometry," *RSC Adv.* **7**(80), 50889–50898 (2017).
38. H. Okabe, P. Splitstone, and J. Ball, "Ambient and source $SO_2$ detector based on a fluorescence method," *J. Air Pollut. Control Assoc.* **23**(6), 514–516 (1973).
39. X. Zhang et al., "Quantitative detection of $SO_2$ produced by $SF_6$ decomposition based on ultraviolet fluorescence method," *Electric Power Autom. Equip.* **38**(6), 177–182 (2018).
40. P. R. Griffths, "Fourier transform infrared spectrometry," *Science* **222**(4621), 297–302 (1983).
41. M. Piemontesi, R. Pietsch, and W. Zaengl, "Analysis of decomposition products of sulfur hexafluoride in negative dc corona with special emphasis on content of $H_2O$ and $O_2$," in *Conf. of the IEEE Int. Symp. on Electrical Insulation*, IEEE, pp. 499–503 (1994).
42. P. Pilzecker, J. I. Baumbach, and R. Kurte, "Detection of decomposition products in $SF_6$: a comparison of colorimetric detector tubes and ion mobility spectrometry," in *Annual Report Conf. on Electrical Insulation and Dielectric Phenomena*, IEEE, pp. 865–868 (2002).
43. W. Ding et al., "Analysis of PD-generated $SF_6$ decomposition gases adsorbed on carbon nanotubes," *IEEE Trans. Dielectr. Electr. Insul.* **13**(6), 1200–1207 (2006).
44. IEC, "Guidelines for the checking and treatment of sulfur hexafluoride ($SF_6$) taken from electrica1 equipment and specification for its re-use," 60480-2004, IEC, Geneva (2004).
45. X. X. Zhang et al., "Infrared spectrum characteristic and discharge trend of $SF_6$ decomposition products," *High Voltage Eng.* **35**(12), 2970–2976 (2009).
46. X. X. Zhang et al., "Recognition of $SF_6$ decomposition components by two-dimensional infrared spectroscopy," *High Voltage Eng.* **36**(6), 1475–1479 (2010).
47. X. X. Zhang et al., "$SF_6$ decomposition components IR measurement and quantify," *Gaodianya Jishu/High Voltage Eng.* **36**(3), 584–589 (2010).
48. X. Zhang et al., "Separating overlapped chromatogram signals of $SF_6$ decomposed products under PD of conductive particles based on curve-fitting," *Trans. China Electrotechn. Soc.* **25**(7), 179–185 (2010).
49. X. Zhang et al., "Research on long optical paths for $SF_6$ partial discharge decomposition components' infrared detection," *Trans. China Electrotech. Soc.* **27**(5), 70–76 (2012).
50. X. Zhang et al., "Fourier transform infrared spectroscopy quantitative analysis of $SF_6$ partial discharge decomposition components," *Spectrochim. Acta Part A* **136**(B), 884–889 (2015).
51. D. C. Dumitraş et al., "Laser photoacoustic spectroscopy: a powerful tool for measurement of trace gases of biological interest at sub-ppb level," *Mol. Cryst. Liq. Cryst.* **418**(1), 217–227 (2004).
52. H. Huszár et al., "Ammonia monitoring at ppb level using photoacoustic spectroscopy for environmental application," *Sens. Actuators B* **134**(2), 1027–1033 (2008).
53. A. Elia et al., "Photoacoustic techniques for trace gas sensing based on semiconductor laser sources," *Sensors* **9**(12), 9616–9628 (2009).
54. A. Pogány, "Photoacoustic instruments for practical applications: present, potentials, and future challenges," *Appl. Spectrosc. Rev.* **46**(1), 1–37 (2015).
55. A. Miklos, P. Hess, and Z. Bozoki, "Application of acoustic resonators in photoacoustic trace gas analysis and metrology," *Rev. Sci. Instrum.* **72**(4), 1937–1955 (2001).
56. T. Lin et al., "Photoacoustic detection of $SF_6$ decomposition by-products with broadband infrared source," in *Int. Conf. on Power System Technology*, IEEE, pp. 1541–1546 (2014).
57. Y. Qiu et al., "Photoacoustic spectroscopy detection of $SOF_2$ characteristic component engendered in $SF_6$ decomposition under partial discharge," *High Voltage Eng.* **39**(5), 1163–1169 (2013).
58. H. Wu et al., "Quartz enhanced photoacoustic $H_2S$ gas sensor based on a fiber-amplifier source and a custom tuning fork with large prong spacing," *Appl. Phys. Lett.* **107**(11), 111104 (2015).
59. A. Varga et al., "Photoacoustic system for on-line process monitoring of hydrogen sulfide ($H_2S$) concentration in natural gas streams," *Appl. Phys. B* **85**(2–3), 315–321 (2006).
60. V. Koskinen et al., "Progress in cantilever enhanced photoacoustic spectroscopy," *Vib. Spectrosc.* **48**(1), 16–21 (2008).
61. V. Koskinen et al., "Cantilever enhanced photoacoustic detection of carbon dioxide using a tunable diode laser source," *Appl. Phys. B* **86**(3), 451–454 (2007).
62. J. Uotila, "A new design of the differential photoacoustic gas detector combined with a cantilever microphone," *Eur. Phys. J. Spec. Top.* **153**(1), 401–404 (2008).
63. X. Zhang, Z. Cheng, and X. Li, "Cantilever enhanced photoacoustic spectrometry: quantitative analysis of the trace $H_2S$ produced by $SF_6$, decomposition," *Infrared Phys. Technol.* **78**, 31–39 (2016).
64. A. O'Keefe and D. A. G. Deacon, "Cavity ring-down optical spectrometer for absorption measurements using pulsed laser sources," *Rev. Sci. Instrum.* **59**(12), 2544–2551 (1988).
65. C. Zhang et al., "CRDS based $SF_6$ decomposition detection technology for $SF_6$ electrical equipment," *South. Power Syst. Technol.* **10**(05), 68–74 (2016).
66. R. S. Brown et al., "Fiber-loop ring-down spectroscopy," *J. Chem. Phys.* **117**(23), 10444–10447 (2002).
67. C. Wang, "Fiber loop ringdown—a time-domain sensing technique for multi-function fiber optic sensor platforms: current status and design perspectives," *Sensors* **9**(10), 7595–7621 (2009).
68. C. Wang and S. T. Scherrer, "Fiber loop ringdown for physical sensor development: pressure sensor," *Appl. Opt.* **43**(35), 6458–64 (2004).
69. A. Yolalmaz et al., "Intracavity gas detection with fiber loop ring down spectroscopy," *Opt. Commun.* **396**, 141–145 (2017).
70. C. Zhu et al., "A method for real-time monitoring of inherent system loss designed for FLRDS-based gas sensors," *IEEE Photonics J.* **8**(5), 1–8 (2016).
71. Y. Zhao, L. Bai, and Q. Wang, "Gas concentration sensor based on fiber loop ring-down spectroscopy," *Opt. Commun.* **309**(22), 328–332 (2013).
72. Y. Zhao et al., "Novel gas sensor combined active fiber loop ring-down and dual wavelengths differential absorption method," *Opt. Express* **22**(9), 11244–11253 (2014).
73. W. Urbanczyk et al., "Photonic crystal fibers for sensing applications," *J. Sens.* **2012**, 1–21 (2012).
74. X. Li et al., "NIR spectrum analysis of natural gas based on hollow-core photonic bandgap fiber," *IEEE Sens. J.* **12**(7), 2362–2367 (2012).

75. J. Wei et al., "Ultra-sensitive all-fibre photothermal spectroscopy with large dynamic range," *Nat. Commun.* **6**, 6767 (2015).
76. H. Lehmann et al., "In-line gas sensor based on a photonic bandgap fiber with laser-drilled lateral microchannels," *IEEE Sens. J.* **11**(11), 2926–2931 (2011).

**Xiaoxing Zhang** received his bachelor's and master's degrees from Hubei Institute of Technology, and doctor's degree from Chongqing University. He is a professor at the School of Electric Engineering, Wuhan University. He is involved in the on-line monitoring and fault diagnosis of high voltage electrical insulation equipment, alternative gases of $SF_6$, the decomposition mechanism of insulating gas $SF_6$, and the new optical sensor.

**Yin Zhang** is a doctoral candidate in School of Electric Engineering, Wuhan University. His research interests include the decomposition mechanism of insulating gas $SF_6$, and the new optical sensor.

Biographies for the other authors are not available.